A COMPARISON OF THE HEIGHT DISTRIBUTIONS OF SOLAR FLARE HARD X-RAYS IN THICK TARGET AND THERMAL MODELS

by

A. Gordon Emslie

National Aeronautics and Space Administration
Gratn NGL 05-020-272

Office of Naval Research
Contract N00014-75-C-0673

SUIPR Report No. 822

October 1980

INSTITUTE FOR PLASMA RESEARCH
STANFORD UNIVERSITY, STANFORD, CALIFORNIA

A COMPARISON OF THE HEIGHT DISTRIBUTIONS OF SOLAR FLARE HARD X-RAYS IN THICK TARGET AND THERMAL MODELS

by

A. Gordon Emslie

National Aeronautics and Space Administration
Grant NGL 05-020-272

Office of Naval Research
Contract N00014-75-C-0673

SUIPR Report No. 822

October 1980

Institute for Plasma Research
Stanford University
Stanford, California

A COMPARISON OF THE HEIGHT DISTRIBUTIONS OF SOLAR FLARE HARD X-RAYS IN THICK TARGET AND THERMAL MODELS

A. Gordon Emslie

Institute for Plasma Research, Stanford University

Received 1980 June 18; accepted 1980 October 20

ABSTRACT

Motivated by recent observations of solar hard X-ray bursts with a spatial resolution of a few arc seconds, we compute the theoretically predicted spatial variation of hard X-ray flux versus height in both thick target non-thermal, and thermal, models of solar hard X-ray bursts. Our work on the thick target model revises previous results in this area by adopting a more realistic model for the flaring atmospheric structure, and also by taking into account energy loss and scattering processes in the evolution of the non-thermal electron beam which have previously been neglected.

It is pointed out that in the so-called "thermal" model currently in vogue, there is a substantial non-thermal bremsstrahlung component at all photon energies; it is further shown that this non-thermal component results in a hard X-ray flux versus height distribution whose maximum brightness per unit length is, similar to the thick target model, located in the chromosphere, and not in the thermal source itself (where the bulk of the total low photon energy bremsstrahlung is emitted). The characteristics of the hard X-ray height distributions in both thick target and thermal models are summarized and compared, and predictions as to the observable spatial structure of the X-ray flare in both cases are made.

Subject Headings: Sun: chromosphere - Sun: corona - Sun: flares - Sun: X-rays

I. INTRODUCTION

Current theoretical models of the hard X-ray bursts commonly associated with solar flares fall into two main classes - thermal and non-thermal. In the former model the X-rays are attributed to collisional bremsstrahlung within an ensemble of thermally relaxed electrons (e.g. Chubb, Kreplin, and Friedman 1966; Brown 1974; Crannell et al. 1978; Mätzler et al. 1978; Brown, Melrose and Spicer 1979; Smith and Lilliequist 1979; Emslie and Brown 1980; Emslie and Vlahos 1980; Smith and Auer 1980; Emslie 1981a). In the latter the X-rays similarly result from bremsstrahlung, although this time from a beam of suprathermal electrons incident on a cold background target. The exact target geometry involved has led to a variety of non-thermal models -- thick target (Brown 1971; Emslie 1980), thin target (Datlowe and Lin 1973), and trap (Takakura and Kai 1966; Brown and Hoyng 1975; Melrose and Brown 1976; Hudson 1978; Emslie, McCaig, and Brown 1979).

Current X-ray spectral measurements (e.g. Hoyng, Brown and van Beek 1976) are unable to distinguish between the various models outlined above, because of the instability of the X-ray spectrum deconvolution problem (e.g. Craig 1979) and because of the ability of a thermal distribution with a non-uniform temperature to mimic a "non-thermal" (e.g., power-law) spectral form (Brown 1974). Similarly, available polarization measurements (Tindo et al. 1970, 1972a, b; Tindo, Mandel'stam, and Shuryghin 1973; Tindo, Shuryghin, and Steffen 1976) are not reliable enough (Mandel'stam 1980) to discriminate amongst the predictions of various models (Brown 1972; Langer and Petrosian 1977; Bai and Ramaty 1978; Emslie and Brown 1980; Leach and Petrosian 1981). It has therefore been suggested (e.g. Rust and Emslie 1979; Emslie and Rust 1980) that spatially resolved hard X-ray images may provide vital clues to aid in the discrimination amongst candidate models.

Observationally, the only "spatially resolved" hard X-ray data published at the time of writing is the fortuitous observation of a behind-the-limb flare by two satellites separated by a suitable distance in ecliptic longitude (Kane et al. 1979). However, with the successful launch of the NASA Solar Maximum Mission satellite, with its Hard X-Ray Imaging Spectrometer (van Beek et al. 1980) on board, there is now an abundance of spatially resolved ($\lesssim$8" resolution) data available for study, and preliminary results have been presented (de Jager et al. 1981; Hoyng et al. 1981).

Theoretically, the only published study of the height distribution of solar hard X-rays in the context of a particular model is by Brown and McClymont (1975), who analyzed the thick and thin target non-thermal models. However, the predicted distribution in these models is a sensitive function of the density structure of the model atmosphere adopted; Brown and McClymont (1975), in making use of a quiet Sun model (Vernazza, Avrett, and Loeser 1973), in fact obtain results which significantly differ from those obtained by using a more realistic flare model atmosphere (Machado and Linsky 1975; Machado et al. 1980); we show this below in §III.

In the present paper we therefore revise Brown and McClymont's (1975) calculations, using a more realistic model atmosphere as a target, and also taking into account the effects of collisional scattering and reverse current ohmic energy losses on the non-thermal electron beam (effects neglected by Brown and McClymont in their analytic calculations). We also compute the height distribution of hard X-rays in the dissipative thermal model (Brown, Melrose, and Spicer 1979; Smith and Lilliequist 1979; Smith and Auer 1980), giving due recognition to the non-thermal high energy tail component in the electron velocity distribution in such models (Brown, Craig, and Karpen 1980; Emslie and Vlahos 1980). The hard X-ray height distribution in coronal trap models (Takakura and Kai 1966; Melrose and Brown 1976) depends on the magnetic

field geometry in the trap and on the electron scattering process within the trap (Melrose and Brown 1976; Wentzel 1976), and will not be dealt with here. In §II we describe the method by which our (numerical) results are obtained. In §III we compare our thick target results with those of Brown and McClymont (1975). In §IV we study the thermal model and show that, contrary to some expectations (Rust and Emslie 1979; Emslie and Rust 1980), the hard X-rays in this model do not have their brightest component in the thermal part of the flaring loop, although the bulk of the total photon flux at low energies emanates from the (larger) thermal region.In §V we discuss the results obtained and show how the two models may be distinguished by spatial measurements with sufficiently high resolution; such spatial resolution is within current instrumental capabilities.

II. METHOD OF COMPUTATION

Since we shall assume the hard X-ray emission from any thermal source to be spatially uniform (see §IV), it remains only to describe the computation of the non-thermal component present in both the thick target and dissipative thermal models. We shall make use of the procedure developed by Emslie (1978, 1980) to compute the dynamics of, and X-ray bremsstrahlung yield from, the beam of non-thermal electrons; we note that his mean scattering and energy loss theory yields results which are very similar to a full Fokker-Planck analysis of the beam-target interaction (Leach and Petrosian 1981).

It has been pointed out by Chambe and Hénoux (1979) that Emslie's (1978) treatment of ion-neutral collisions neglects the inelastic momentum loss from the charged beam particles. This loss is given by

$$\left.\frac{dv_{||}}{dt}\right|_{inelastic} = \frac{1}{mv_{||}}\frac{dE}{dt} \quad , \tag{1}$$

where $v_{||}$ is the component of velocity in the precollision direction, and m and E the beam particle mass and energy respectively. Adding these inelastic momentum loss terms to Emslie's (1978) equation (22) gives the revised total momentum loss rate in a target of arbitrary ionization level:

$$\frac{dv_{||}}{dt} = -\frac{\pi e^4}{E^2}\left\{ x\,\Lambda\left(2 + \frac{m}{m_p} + \frac{m}{m_e}\right) + (1-x)\left[\frac{m_p}{(m_p+m)}\Lambda'' + \left(\frac{m}{m_e}\right)\Lambda'\right]\right\} \quad . \tag{2}$$

In this equation m_e and m_p are the electron and proton masses respectively, e (e.s.u.) is the electronic charge, x is the fractional ionization

number of hydrogen, and Λ, Λ', Λ'' are Coulomb logarithms, defined in Emslie's (1978) paper. It follows that Emslie's (1978) equation (25) for the scattering parameters β should read

$$\beta_e = \frac{2x\Lambda + (1-x)\,\Lambda''}{\Lambda' + x\,(\Lambda-\Lambda')} \quad ; \quad \beta_p = 0 \qquad (3)$$

(β_e and β_p corresponding to electron and proton bombardment respectively). In turn, equation (14) of Emslie (1980), which includes the effect of both collisions and reverse current ohmic energy and momentum losses from the beam electrons, should read

$$\frac{d\mu}{dN} = -\left\{\frac{\pi e^4}{E^2}\left[2x\Lambda + (1-x)\,\Lambda''\right] + \frac{\eta e^2 F_{oo}\,(1-\mu^2)}{2n\mu E}\left(1 + \frac{E_o^*}{E_{oo}}\right)^{1-\delta}\right\}, \qquad (4)$$

where μ is the direction cosine (w.r.t. the vertical) of the beam electrons, n and η are the plasma density (cm^{-3}) and resistivity (e.s.u.) respectively, E_o^* is the minimum injection energy required of an electron to penetrate to a column depth N (cm^{-2}), and F_{oo}, E_{oo} and δ define the injected electron flux spectrum:

$$F_o(E_o)\ (\text{electrons cm}^{-2}\text{s}^{-1}\text{keV}^{-1}) = (\delta-1)\,F_{oo}\,E_{oo}^{\delta-1}\,(E_{oo}+E_o)^{-\delta}\ . \qquad (5)$$

Note that Emslie's (1980) equation (13) remains unaltered.[1]

[1] We have re-performed Emslie's (1980) calculations using the revised version of his equations (13) and (14) and find no significant changes from his results.

Using the revised equations as outlined above, we may now derive the variation of electron flux with depth in the target, and so compute the X-ray bremsstrahlung yield as a function of depth and photon energy (see Emslie's [1980] equation [22]). Emslie (1980) integrated this over depth to obtain

the resulting bremsstrahlung spectrum only; however, it is a straightforward matter to use his results directly to compute the height variation of the X-ray flux at a given photon energy. Results follow in the next two sections.

III. RESULTS FOR THE THICK TARGET MODEL

As mentioned in §I, the earlier treatment of this problem by Brown and McClymont (1975) uses the quiet Sun atmospheric density structure (Vernazza, Avrett, and Loeser 1973) as a target. This structure in fact bears little resemblance to that found in flares (Machado and Linsky 1975; Lites and Cook 1979; Machado et al. 1980). The principal difference between the quiet Sun and flare model atmospheres is the particle column depth N_{TZ} (cm^{-2}) of the transition zone, with its associated steep density gradient; in empirical flare model atmospheres $N_{TZ} \approx 10^{21} cm^{-2}$, while N_{TZ} is $\approx 2 \times 10^{18} cm^{-2}$ in the quiet Sun (Vernazza, Avrett, and Loeser 1973) and $\approx 3 \times 10^{19} cm^{-2}$ in active regions (Basri et al. 1979). It is not immediately obvious whether one should employ an active region or flare empirical model as a target for the bremsstrahlung-producing non-thermal electrons, since they are flash-phase phenomena and empirical flare modeling to date (e.g. Machado and Emslie 1979; Machado et al. 1980) applies only to the later stages of the flare. However, since in a thick target model the principal cause of the increase in N_{TZ} is the bombardment by the bremsstrahlung-producing electrons, and since it is easily shown that preflare chromospheric material rises in temperature by the required 10^7K or so in a very short time (see eq. [8] of Emslie and Noyes 1978), it seems more reasonable to use the flare models of Machado et al. (1980) as a background target for our computations. (For further discussion of the validity of empirical flare model atmospheres, see Emslie, Brown, and Machado 1981.) Now, the predicted height distribution of thick target hard X-rays is a combination of two effects: (i) density variation (the thick target yield is proportional to the ambient number density), and (ii) electron flux attenuation (the yield is also proportional to the electron flux at a given level, which is in turn a decreasing function of the column

density). Thus one sees that by moving the level at which the large photon flux enhancement occurs due to effect (i) to a larger (flare) value of the column density N (and so to a level at which the electron flux has attenuated to a much higher degree), a significant difference from Brown and McClymont's (1975) predicted X-ray flux versus column density profile may result.

In addition to these considerations, we note that Brown and McClymont (1975) neglect collisional scattering of the beam electrons, and also reverse current ohmic energy losses from the beam; these processes can result in substantial modifications to the electron flux versus depth profile (Emslie 1980). Further, Brown and McClymont's (1975) assumption of a fully ionized target underestimates the bremsstrahlung yield at greater depths, where the fractional ionization level of hydrogen is small (Brown 1973). All these effects are incorporated in the present treatment.

We have calculated the variations of hard X-ray flux versus depth for two model atmospheres. The first uses the model chromosphere 'F1' of Machado et al. (1980) and the second the model chromosphere 'F2' of these authors (hereafter these models will be referred to as MAVN1 and MAVN2 respectively). To these models we attached isothermal coronae (temperature 3×10^7 K) 3×10^4km in length (measured down one half of the loop). The density at the loop apex was taken to be $3 \times 10^{10} cm^{-3}$ for model MAVN1 and $10^{11} cm^{-3}$ for model MAVN2, and the density variation along the coronal part of the loop was taken to be smoothly increasing with depth such that the integrated column density N_{TZ} at the transition zone matched Machado et al.'s (1980) values of 1.5×10^{20} cm^{-2} and 1.6×10^{21} cm^{-2} respectively. These coronal models are admittedly somewhat crude; however, it turns out that the coronal hard X-ray emission per unit length in the thick target model is negligible compared to that in the chromosphere (Figures 1 and 2), so that any deficiencies in the

the model adopted will not significantly affect the conclusions of the paper.

Figure 1 In Figures 1 and 2 we show the variation of ϕ, the fraction of the total X-ray flux emitted per km of vertical distance at depth z (km) (column depth N $[cm^{-2}]$), for these two flare models. The electrons were assumed to be injected by a "black box" mechanism (with no intrinsic hard X-ray signature) at the top of the coronal loop (N=0) with a flux spectrum given by equation (5) with $F_{oo} = 10^{19}$ electrons $cm^{-2}s^{-1}$, $E_{oo} = 20$ keV, and $\delta = 4$ (see Emslie 1980). The dashed line indicates a purely collisional calculation of the electron beam dynamics and the solid line a calculation involving reverse current losses as well. These reverse current losses are quite sensitive to the atmospheric model adopted, particularly in the corona (Emslie 1980), which is why we show the purely collisional calculation for comparison, even though it is unphysical. Note also that the requirement that the reverse current be stable to current-driven plasma turbulence sets an upper limit to the significance of reverse current ohmic dissipation in the electron beam energetics. Only for certain coronal conditions (e.g. high density, approximately equal electron and ion temperatures) is such a large flux F_{oo} allowed to pass stably; if these conditions are not met then F_{oo} must be reduced and the effects of reverse currents correspondingly decreased (Emslie 1981b). Note finally that the figures only extend down to a depth $N = 10^{22}$ cm^{-2}. This is the thermalization depth of electrons with initial (i.e. injected) energy $\tilde{\sim}300$ keV (e.g. Emslie 1978); since data on hard X-rays with photon energies of this order are poor, we consider extrapolation to higher electron energies (and so greater depths) than this highly uncertain. If the spectrum (5) does in fact extend to arbitrarily large energies E_o, then $\phi(N)$ will asymptotically approach a power-law form with index $(1-\delta)/2 = -1.5$ (Brown and McClymont 1975; Emslie 1978).

Figure 2 It is evident from the figures that the effect of reverse current ohmic dissipation is significant for the coronal region of model MAVN1 only; this is due to the relatively low coronal densities and consequently small collisional losses (compared to ohmic ones) in this region (Emslie 1980). Note that the effect of the reverse current is to enhance the coronal component of the hard X-ray emission relative to the chromospheric component. In fact (see Emslie 1980), both chromospheric and coronal components are reduced (in absolute flux units) from their purely collisional values; however the effect is more severe on the chromospheric emission due to the reduction in flux penetrating to large depths effected by the reverse current ohmic dissipation in the corona.

Comparing our results to those of Brown and McClymont (1975) we notice that in model MAVN2 (Figure 2) the region of brightest X-ray emission per unit length is narrower than in either Brown and McClymont's (1975) results or the results for model MAVN1 (Figure 1) and is located at the base of the transition region, as opposed to mid-way into the chromosphere. This is because, as remarked above, the transition zone level in model MAVN2 is so deep that the electron beam has already significantly attenuated before it reaches the chromosphere, to such an extent that the increase of chromospheric density with depth from the base of the transition zone downwards cannot overcome this diminishing flux effect. In the quiet Sun and MAVN1 models, however, this coronal attenuation is not so significant, and consequently the region of maximum bremsstrahlung yield per unit length is pushed downwards into the chromosphere and made broader.

These differences are, however, probably quite undistinguishable by observation, at the current level of instrument capability. The height range over which $\phi \gtrsim 0.1\phi_{max}$ is $\simeq 2\times10^3$ km (3" in angle) for Brown and

McClymont's quiet Sun calculation (see their Figure 4), $\approx 10^3$ km (1½") for model MAVN1 (Figure 1), and $\approx 5 \times 10^2$ km (1") for model MAVN2 (Figure 2). All of these angular sizes are below the currently available spatial resolution of hard X-ray detectors (van Beek et al. 1980).

It is worth commenting further on the results for model MAVN2. Figure 2 shows that the depth dependence of hard X-ray emission in the coronal part of the loop is significantly different for low ($\varepsilon \simeq 10$ keV) and high ($\varepsilon \simeq 70$ keV) photon energies. For low energies the principal cause of the decrease of ϕ with depth is effect (ii) above, namely electron flux attenuation, while for high energies effect (i) (increasing density with depth) dominates, causing the X-ray flux per unit length to increase with depth. One would expect effect (ii) to begin to dominate effect (i) (causing a maximum in ϕ) when one reaches the depth at which electrons of energy $E \gtrsim \varepsilon$ begin to lose energy rapidly (note the dependence of the Bethe-Heitler bremsstrahlung cross-section [Heitler 1954] on electron energy E). This occurs when $(\varepsilon\,[\mathrm{keV}])^2 \lesssim 6\pi e^4 \Lambda N \simeq (N/10^{17})$ (Emslie 1978); the curve for $\varepsilon = 40$ keV in Figure 2 has a maximum at $N \simeq 3 \times 10^{20}$ cm^{-2}, in good agreement with this prediction.

This concludes our discussion of the thick target model. In the next section we shall consider the thermal model, and compare the results from the two models in § V.

IV. RESULTS FOR THE THERMAL MODEL

In this section we investigate the height distribution of hard X-rays expected in the "dissipative thermal" model, originally proposed by Brown, Melrose, and Spicer (1979), and currently under extensive investigation (see Smith and Lilliequist 1979; Emslie and Brown 1980; Emslie and Vlahos 1980; Smith and Auer 1980; Smith and Brown 1980; Emslie 1981a). This model is characterized by a "thermal" distribution of electrons at the top of a coronal loop, confined parallel to the loop axis by a strong magnetic field and perpendicular to the loop axis by a pair of collisionless ion-acoustic turbulent fronts, which result from the instability of the reverse current associated with the outward heat flux from the source (see, e.g. Kahler 1975) and which move along the arch at approximately the local ion-sound speed (Smith and Lilliequist 1979; Smith and Auer 1980).

It was recognized by Brown, Melrose, and Spicer (1979) and by Vlahos and Papadopoulos (1979) that in such a model very high energy electrons are not confined by the turbulent plasma fronts and escape downwards in much the same manner as a thick target beam. Although the exact details of this escape process are somewhat uncertain (Smith and Brown 1980), it is typically found that all electrons with velocities $v \gtrsim 3\, v_e$ (where v_e is the mean electron thermal velocity) can escape. Brown, Craig, and Karpen (1980) and Emslie and Vlahos (1980) have considered the thick target bremsstrahlung yield from these high energy electrons and find that it is comparable to the thermal yield for photon energies ε greater than a few times $\frac{1}{2}m_e v_e^2$ (the mean electron thermal energy). Specifically, Emslie and Vlahos (1980) give the ratio of thick target to thermal bremsstrahlung at photon energy ε as

$$\eta(\varepsilon) = \begin{cases} \dfrac{6.6\times10^{11}}{nL}\,\dfrac{\beta^4}{4(\delta-2)}\; e^{-\beta^2/2}\, e^{\varepsilon/kT}\,(kT)^2\,\ln\left(\dfrac{2\beta^2 kT}{\varepsilon}\right) & ;\ \varepsilon < E_{min} \\ \infty & ;\ \varepsilon \geq E_{min} \end{cases}, \qquad (6)$$

where k is Boltzmann's constant, β the ratio of the critical escape velocity to v_e and δ the spectral index of the power-law escaping tail (see Emslie and Vlahos 1980); note that assuming the tail to be a simple extended Maxwellian [see Brown, Craig, and Karpen 1980] only reduces η by a factor of $\lesssim 2$ for the parameter set considered and so does not affect the conclusions to follow. n (cm^{-3}), T(K), and L(km), are the density, electron temperature, and length of the thermal source and E_{min} is the threshold energy for an electron to escape through the conduction fronts $= \frac{1}{2}\beta^2 kT$. We shall hereafter consider a source model with $\beta = 3$, $\delta = 4$, $n = 10^{11}$ cm^{-3} (see Smith and Lilliequist 1979; § III) and $T = 22.2$ keV (so that the electron escape energy threshold E_{min} is 100 keV); results for other values of these parameters can readily be obtained using equations (6) and (8). For the parameter set chosen,

$$\eta(\varepsilon) = \frac{369}{L} \exp\,(0.045\,\varepsilon) \ln\left(\frac{400}{\varepsilon}\right) \qquad (7)$$

(with ε measured in keV); this is shown graphically in Figure 3.

Figure 3

If we assume that the thermal bremsstrahlung emission is spatially uniform over $z < z^*$ ($N < N^*$), then the fractional (relative to the combined thermal plus thick target non-thermal emission in one leg of the arch) yield per km of loop is

$$\phi(\varepsilon, z) = \begin{cases} \dfrac{2 + \eta(\varepsilon)\phi_{tt}(\varepsilon, z)L}{[1 + \eta(\varepsilon)]L} & ;\ z < z^* \\ \dfrac{\eta(\varepsilon)\phi_{tt}(\varepsilon, z)}{1 + \eta(\varepsilon)} & ;\ z > z^* \end{cases} \qquad (8)$$

where $\phi_{tt}(\varepsilon, z)$ is the thick target fractional yield as found in §III, but with a lower cutoff of 100 keV introduced to the spectrum (5).

Figure 4

In Figure 4 we show the resulting $\phi(z)$ structures for various ε; results for the thick target model neglecting reverse currents (see Figure 2) are shown

for comparison. Model MAVN2 was used in the calculations; the results using model MAVN1 are similar. The column density N^* was taken to be 10^{20} cm^{-2} and the corresponding source length 2×10^9 cm (note the symmetry in the source model). Note that the ratio of thick target to thermal values of ϕ in the model is in fact independent of L : to see this we rewrite equation (7) as

$$\eta(\varepsilon) = \frac{\eta_o(\varepsilon)}{L} \quad , \tag{9}$$

with

$$\eta_o(\varepsilon) = 369 \exp\,(0.045\ \varepsilon)\ln\left(\frac{400}{\varepsilon}\right) \cdot \tag{10}$$

Then equation (8) becomes

$$\phi(\varepsilon,z) = \begin{cases} \dfrac{2 + \eta_o(\varepsilon)\phi_{tt}\ (\varepsilon,z)}{L + \eta_o(\varepsilon)} & ;\ z < z^* \\ \dfrac{\eta_o(\varepsilon)\phi_{tt}\ (\varepsilon,z)}{L + \eta_o(\varepsilon)} & ;\ z > z^* \end{cases} \tag{11}$$

so that the ratio of ϕ values in the "chromospheric" and "thermal" parts of the source is

$$\theta(\varepsilon) = \frac{\eta_o(\varepsilon)[\phi_{tt}\ (\varepsilon,z)]_{\text{chromosphere}}}{2 + \eta_o(\varepsilon)[\phi_{tt}\ (\varepsilon,z)]_{\text{thermal region}}} \cdot \tag{12}$$

Since for all values of ε the second term in the denominator is negligible compared to unity (the suprathermal electrons give off little bremsstrahlung in the relatively tenuous coronal plasma - note the sharp drop off in ϕ at $z > z^*$ - Figure 4), we see that $\theta(\varepsilon)$ is, to a good approximation, constant:

$$\theta(\varepsilon) = \frac{\eta_o(\varepsilon)[\phi_{tt}(\varepsilon,z)]_{\text{chromosphere}}}{2} \quad . \qquad (13)$$

It is immediately evident from Figure 4 that the maximum bremsstrahlung yield per unit length at all energies still occurs at the base of the transition region. This is contrary to earlier speculations (e.g. Rust and Emslie 1979; Emslie and Rust 1980) that the most intense hard X-ray emission should be emitted in the thermal region at the top of the arch. Comparison of the thick target and thermal model results in Figure 4 shows that the fractional contribution from the coronal region is indeed enhanced in the thermal model; however this is not at the expense of the chromospheric emission but rather at the expense of the emission in the region between the conduction fronts and the transition region (i.e. between $z = -2 \times 10^4$ km and $z = 0$).[2]

[2] Note that $\phi(z)$ is an increasing function of z for all energies in this region of the atmosphere; only when N reaches $\simeq 10^{21} cm^{-2}$, the thermalization depth for electrons of energy $E_{min} = 100$ keV, does any significant decrease in ϕ occur; cf. discussion of thick target model curves in § III.

This behavior is in fact easily understood: since the electron energy required to penetrate to chromospheric depths in model MAVN2 is $\gtrsim 80$ keV (see, e.g., Emslie 1978), the fractional chromospheric yield in the thick target model is matched in the thermal model by the contribution from the high energy escaping tail. Further, due to the high background plasma density in the chromosphere, the high energy tail thermalizes in a very short distance and also has a high bremsstrahlung yield per unit length (the additional fact that the chromospheric plasma is only partially ionized further enhances the chromospheric emission - see Brown 1973). However, in the tenuous coronal plasma between the confining turbulent conduction fronts and the transition region, the thick target component, being inefficient compared to thermal emission at these densities (Smith and Lilliequist 1979; Smith and Auer 1980) is very

small. We thus see that the height distribution of hard X-rays in the dissipative thermal model is characterized by two very low intensity regions, one in each leg of the flaring loop, flanked above and below by relatively bright regions, making five regions in all. The more intense of these bright regions are the lower ones, with the degree of contrast between them and the uppermost region increasing with increasing photon energy (see Figure 4).

V. DISCUSSION

The principal result of the above analysis is that the brightest hard X-ray region is always at the base of the transition zone, in both thick target and thermal models. This result follows in the thick target model because of the use of a more realistic model atmosphere than previously employed (cf. the results of Brown and McClymont 1975), and in the thermal model because of the presence of a precipitating high energy non-thermal tail of electrons, which behave exactly as a thick target beam.

In our discussion of the thermal model (§IV) we have tacitly assumed that the high energy tail is always present (i.e. we have assumed a steady-state situation). Processes by which this escaping tail may be repopulated from the bulk thermal plasma are not well understood (see Emslie and Vlahos 1980; Smith and Brown 1980) and so it must be conceded that perhaps the X-ray height distribution depicted in Figure 4 strictly applies only to an initial transient state. In such a case the "relaxed" ϕ distribution would simply be a rectangle of length L/2 and height 2/L (see Figure 4). Clearly whether or not the high energy tail is continuously repopulated is of crucial importance; for the present we note that the interpretation of microwave bursts by Emslie and Vlahos (1980) in the context of the dissipative thermal model demands that the tail <u>does</u> exist.

Returning to the results of Figure 4, we note that the distribution will in fact be time-dependent, as the conduction fronts advance along the arch (recall, however, the results of § IV [equation (12)], which showed that this variation of L does not affect the dominance of the chromospheric component in the $\phi[z]$ profile). An obvious corollary to this is that the source has only a finite lifetime $\tau \gtrsim L_{TZ}/c_s$, where L_{TZ} is the distance from the energy release point to the transition zone

and c_s is the ion sound speed $\approx 10^4 T^{\frac{1}{2}}$ cm s^{-1} . For plausible parameters we see that τ is of order 30 seconds, which is somewhat greater than the time resolution of available hard X-ray imaging instruments (van Beek et al. 1980). Thus it appears that the introduction of a "multiple kernel model", such as has been advocated by Brown, Craig, and Karpen (1980) to explain observed (Mätzler et al. 1978) emission measure/temperature correlations (see, however, Emslie 1981a) may be unnecessary. (Note, however, that even if such a multiple kernel model were appropriate,with the kernels all formed near the top of the arch, we should replace L by a mean $\bar{L}$ in the analysis of §IV, thereby resulting in a distribution very similar to that of Figure 4 [recall the insensitivity of the results to L -- §IV]).

Finally we note that the best spatial resolution currently available in the hard X-ray spectral region is rather limited ($\gtrsim$ 8" ; van Beek et al. 1980). An angular resolution of this order corresponds to a length of $\approx$ 5000 km on the solar surface, implying that we should really scan Figures 1, 2, and 4 with a rather broad "filter" of this width. The effect of this smoothing depends on whether we are considering thermal or non-thermal models, and on the model atmosphere adopted. For instance, for the thick target model with atmosphere MAVN1 (Figure 1), one coronal "pixel" will contain some $10^{-5} \times 5 \times 10^3 \approx 5\%$ of the emission, while a chromospheric pixel will contain some 70% of the total emission (from one leg of the arch). Thus in this case we should expect to see two chromospheric "bright points" at the feet of the flare loop, with little emission elsewhere.

In the thick target model with atmosphere MAVN2, we find that, due to the greater amount of coronal material compared to atmosphere MAVN1, a coronal pixel now observes some 15% of the emission (at $\varepsilon \approx 40$ keV), while the chromospheric pixel observes a similar fraction of the total emission. Thus we should here expect to see almost uniform emission over the whole loop.

Finally, in the thermal model, we see that a pixel observing the thermal region will contain some 30-40% of the emission, a chromospheric pixel will observe some 20-30%, and a pixel in the region between the thermal region and the transition zone will observe at most 2 or 3 percent of the emission. In this case we therefore expect to see the characteristic "five layer" structure mentioned in § IV.

These observational predictions are sufficiently distinct to distinguish between the above three scenarios with currently available instrumentation (van Beek et al. 1980), and it is hoped that results from the Solar Maximum Mission Hard X-Ray Imaging Spectrometer will be able to cast some light upon which scenario actually applies to solar flares.

I thank J. Leach and P.A. Sturrock for their comments on the manuscript and help in clarifying the presentation, and the referee for his excellent criticism of the original manuscript. This research was supported by NASA Grant NGL 05-020-272 and ONR Contract N00014-75-C-0673.

REFERENCES

Bai, T., and Ramaty, R., 1978, Ap. J., 219, 705.

Basri, G.S., Linsky, J.L., Bartoe, J. -D., Brueckner, G.E., and van Hoosier, M.E., 1979, Ap.J., 230, 924.

Brown, J.C. 1971, Solar Phys., 18, 489.

_____. 1972, Solar Phys., 26, 441.

_____. 1973, Solar Phys., 28, 151.

_____. 1974, in IAU Symposium 57, Coronal Disturbances, ed. G.A. Newkirk, Jr. (Dordrecht: Reidel), p. 395.

Brown, J.C., Craig, I.J.D., and Karpen, J.T. 1980, Solar Phys., 67, 143.

Brown, J.C., and Hoyng, P. 1975, Ap. J., 200, 734.

Brown, J.C., and McClymont, A.N. 1975, Solar Phys., 41, 135.

Brown, J.C., Melrose, D.B., and Spicer, D.S. 1979, Ap. J., 228, 592.

Chambe, G., and Hénoux, J.-C. 1979, Astr. Ap., 80, 123.

Chubb, T.A., Kreplin, R.W., and Friedman, H. 1966, J. Geophys. Res. 71, 3611.

Craig, I.J.D., 1979, Astr. Ap., 79, 121.

Crannell, C.J., Frost, K., Mätzler, C., Ohki, K., and Saba, J.L. 1978, Ap. J., 223, 620.

Datlowe, D.W., and Lin, R.P. 1973, Solar Phys., 32, 459.

de Jager, C., et al. 1981, Ap. J. (Letters), in press.

Emslie, A.G. 1978, Ap. J., 224, 241.

_____. 1980, Ap. J., 235, 1055.

_____. 1981a, Ap. J., 243, in press.

_____. 1981b, Ap. J.(Letters), to be submitted.

Emslie, A.G., and Brown, J.C. 1980, Ap. J., 237, 1015.

Emslie, A.G., Brown, J.C., and Machado, M.E. 1981, Ap. J., submitted.

Emslie, A.G., McCaig, M.G., and Brown, J.C. 1979, Solar Phys., 63, 175.

Emslie, A.G., and Noyes, R.W. 1978, Solar Phys., 57, 373.

Emslie, A.G., and Rust, D.M. 1980, Solar Phys., 65, 271.

Emslie, A.G., and Vlahos, L. 1980, Ap. J., 242, in press.

Heitler, W. 1954, The Quantum Theory of Radiation (Oxford: Oxford University Press).

Hoyng, P., Brown, J.C., and van Beek, H.F. 1976, Solar Phys., 48, 197.

Hoyng, P., et al. 1981, Ap. J. (Letters), in press.

Hudson, H.S. 1978, Ap. J., 224, 247.

Kahler, S.W. 1975, in IAU Symposium 68, Solar Gamma, X-, and EUV Radiation, ed. S.R. Kane (Dordrecht: Reidel), p. 211.

Kane, S.R., Anderson, K.A., Evans, W.D., Klebesadel, R.W., and Laros, J. 1979, Ap. J.(Letters), 233, L151.

Langer, S.H., and Petrosian, V. 1977, Ap. J., 215, 666.

Leach, J., and Petrosian, V. 1981, Ap. J., to be submitted.

Lites, B.W., and Cook, J.W. 1979, Ap. J., 228, 598.

Machado, M.E., Avrett, E.H., Vernazza, J.E., and Noyes, R.W. 1980, Ap. J., 242, in press.

Machado, M.E., and Emslie, A.G. 1979, Ap. J., 232, 903.

Machado, M.E., and Linsky, J.L. 1975, Solar Phys., 42, 395.

Mandel'stam, S.L. 1980, seminar, University of California at San Diego, January.

Mätzler, C., Bai, T., Crannell, C.J., and Frost, K.J. 1978, Ap. J., 223, 1058.

Melrose, D.B., and Brown, J.C. 1976, M.N.R.A.S., 176, 15.

Rust, D.M., and Emslie, A.G. (eds.) 1979, Energy Release in Solar Flares, UAG-72 (Boulder: World Data Center A).

Smith, D.F., and Auer, L.H. 1980, Ap. J., 238, 1126.

Smith, D.F., and Brown, J.C. 1980, Ap. J., 242, in press.

Smith, D.F., and Lilliequist, C.G. 1979, Ap. J., 232, 582.

Takakura, T., and Kai, K. 1966, Pub. Astr. Soc. Japan, 18, 57.

Tindo, I.P., Ivanov, V.D., Mandel'stam, S.L., and Shuryghin, A.I. 1970, Solar Phys., 14, 204.

_____ . 1972a, Solar Phys., 27, 426.

Tindo, I.P., Ivanov, V.D., Valníček, B., and Livshits, M.A. 1972b, Solar Phys., 27, 426.

Tindo, I.P., Mandel'stam, S.L., and Shuryghin, A.I. 1973, Solar Phys., 32, 469.

Tindo, I.P., Shuryghin, A.I., and Steffen, W. 1976, Solar Phys., 46, 219.

van Beek, H.F., Hoyng, P., Lafleur, B., and Simnett, G.M. 1980, Solar Phys. 65, 39.

Vernazza, J.E., Avrett, E.H., and Loeser, R. 1973, Ap. J., 184, 605.

Vlahos, L., and Papadopoulos, K. 1979, Ap. J., 233, 717.

Wentzel, D.G. 1976, Ap. J., 208, 595.

FIGURE CAPTIONS

Figure 1: Fraction of total thick target bremsstrahlung yield ϕ (km^{-1}) versus depth z (km) and column depth N (cm^{-2}) for photon energies 10, 40, and 70 keV with model atmosphere MAVN1 (Machado et al. 1980) as background. The z-coordinate is measured from the transition zone downwards; note the different scale in the coronal and chromospheric regions of the figure. The solid curves include the effects of both collisional and reverse current ohmic losses from the bremsstrahlung-producing non-thermal electron beam; the dashed line takes into account only collisional losses. Compare with Figure 2 and with Figure 3 of Brown and McClymont (1975).

Figure 2: As for Figure 1, except using atmospheric model MAVN2 (Machado et al. 1980) as background. Since MAVN2 has a deeper transition zone than MAVN1 the electron flux has already been significantly attenuated by the time it reaches the transition zone; thus the region of maximum bremsstrahlung yield per unit length is very localized and occurs at the base of the transition zone. This result is markedly different to the results of Brown and McClymont (1975), due to their adoption of an unrealistic (quiet Sun) background atmosphere.

Figure 3: Ratio of thick target to thermal hard X-ray bremsstrahlung (η) as a function of photon energy ϵ in the "thermal" model discussed in §IV. Above the electron escape energy threshold of 100 keV there is insignificant thermal emission and η becomes infinite. Note the substantial contribution of the thick target emission at all energies; this has important implications for the height structure of hard X-rays in this model (see §IV and

Figure 4).

Figure 4: ϕ versus N for thermal model with parameter set outlined in §IV. The figure is normalized so that $\int \phi dz$ is unity for one leg of the arch. The hard X-ray flux versus height structure is characterized by two dark regions (one in each leg of the arch), flanked outside and in between by bright regions. Note that the ϕ (N) structure is time dependent due to the motion of the conduction fronts through the corona, although this does not affect the relative sizes of ϕ values in the corona and chromosphere (see §IV).

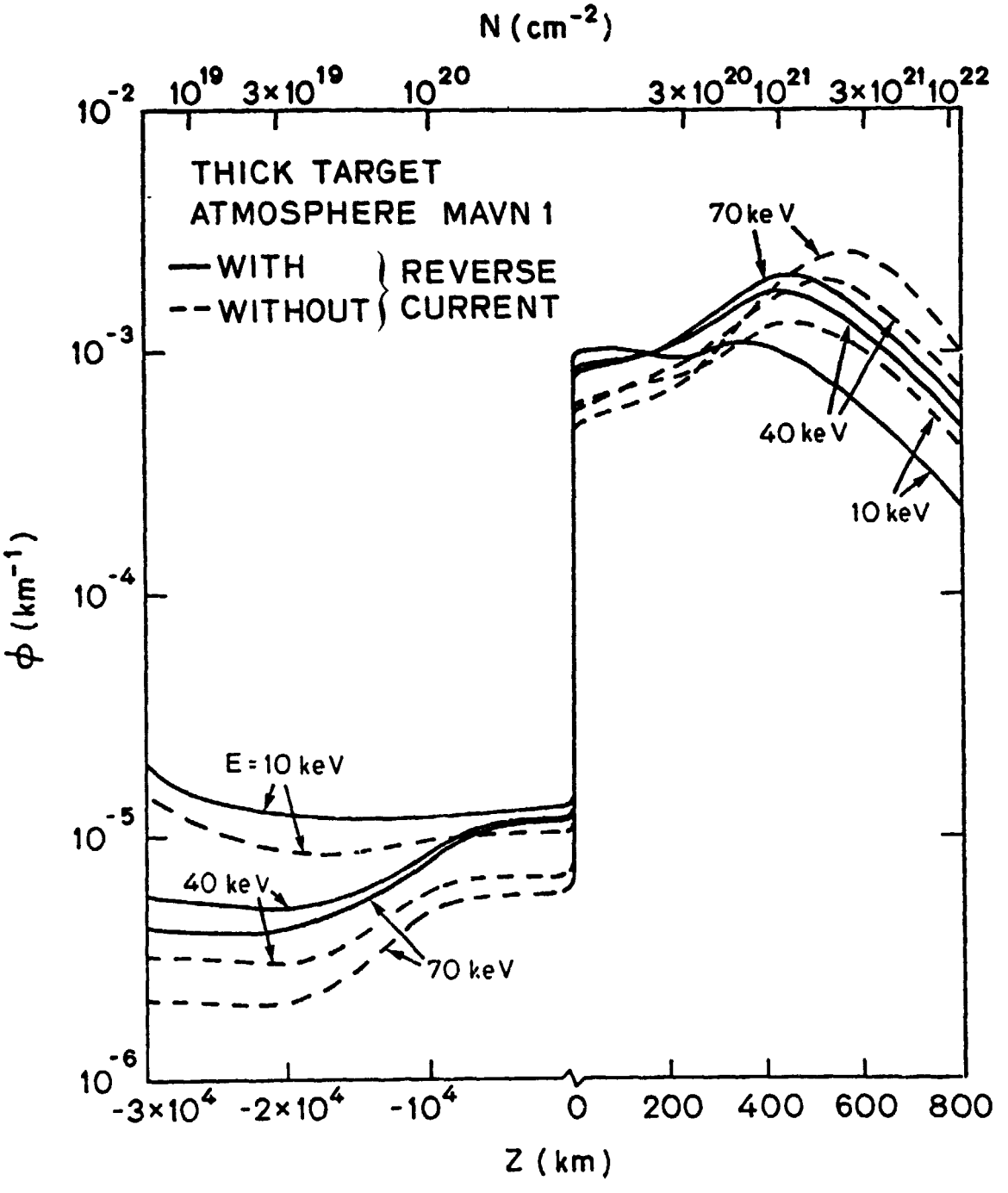
N (cm^{-2})
10^{19} 3×10^{19} 10^{20} 3×10^{20} 10^{21} 3×10^{21} 10^{22}
10^{-2}
THICK TARGET
ATMOSPHERE MAVN 1
—WITH
--WITHOUT
REVERSE CURRENT
70 keV
40 keV
10 keV
E = 10 keV
40 keV
70 keV
10^{-3}
10^{-4}
10^{-5}
10^{-6}
ϕ (km^{-1})
-3×10^{4} -2×10^{4} -10^{4} 0 200 400 600 800
Z (km)

Figure 1

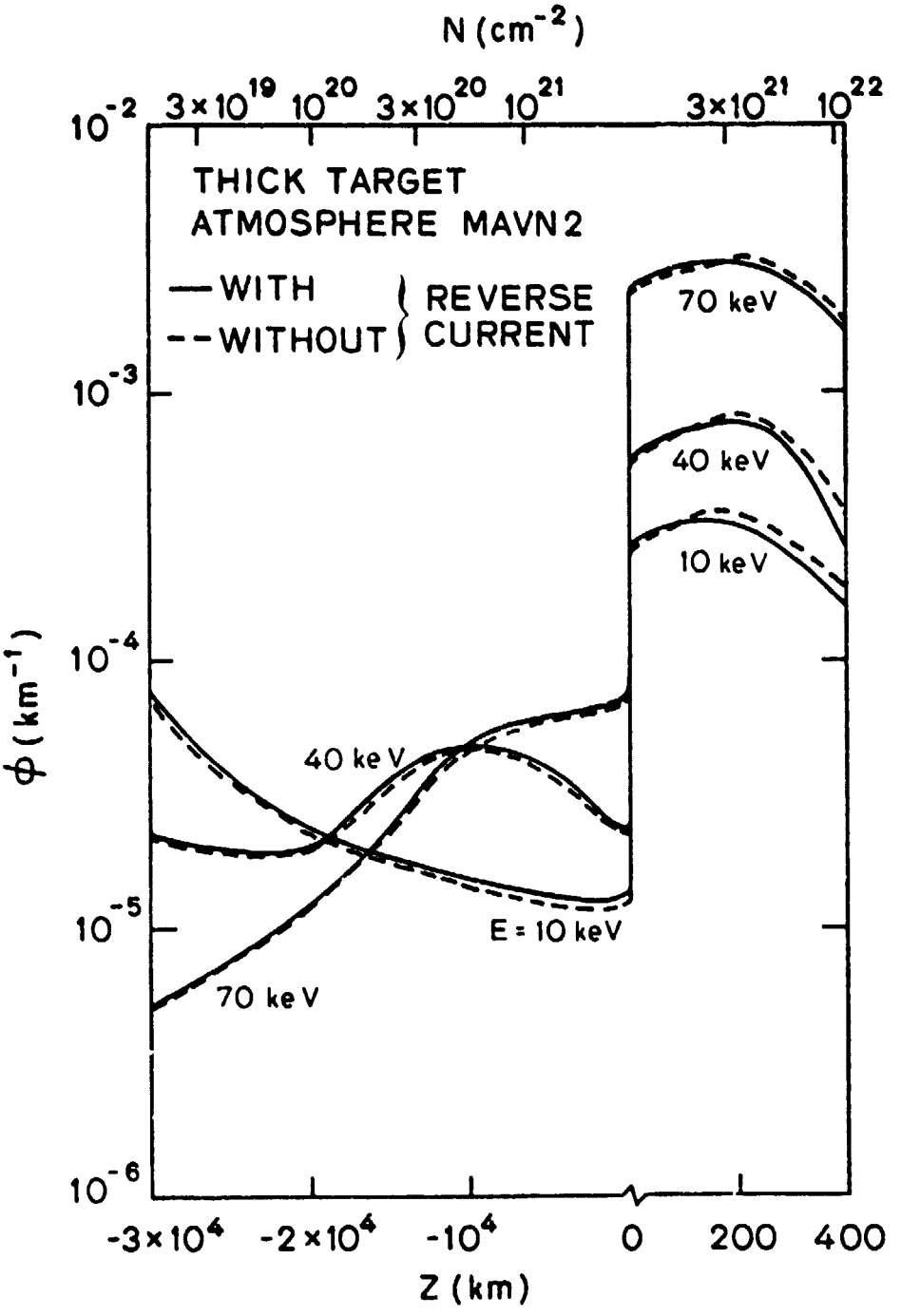
N (cm^{-2})
10^{-2}
3×10^{19}
10^{20}
3×10^{20}
10^{21}
3×10^{21}
10^{22}
THICK TARGET
ATMOSPHERE MAVN2
—WITH
--WITHOUT
REVERSE CURRENT
70 keV
40 keV
10 keV
10^{-3}
10^{-4}
10^{-5}
10^{-6}
ϕ (km^{-1})
40 keV
E = 10 keV
70 keV
-3×10^{4}
-2×10^{4}
-10^{4}
0
200
400
Z (km)

Figure 2

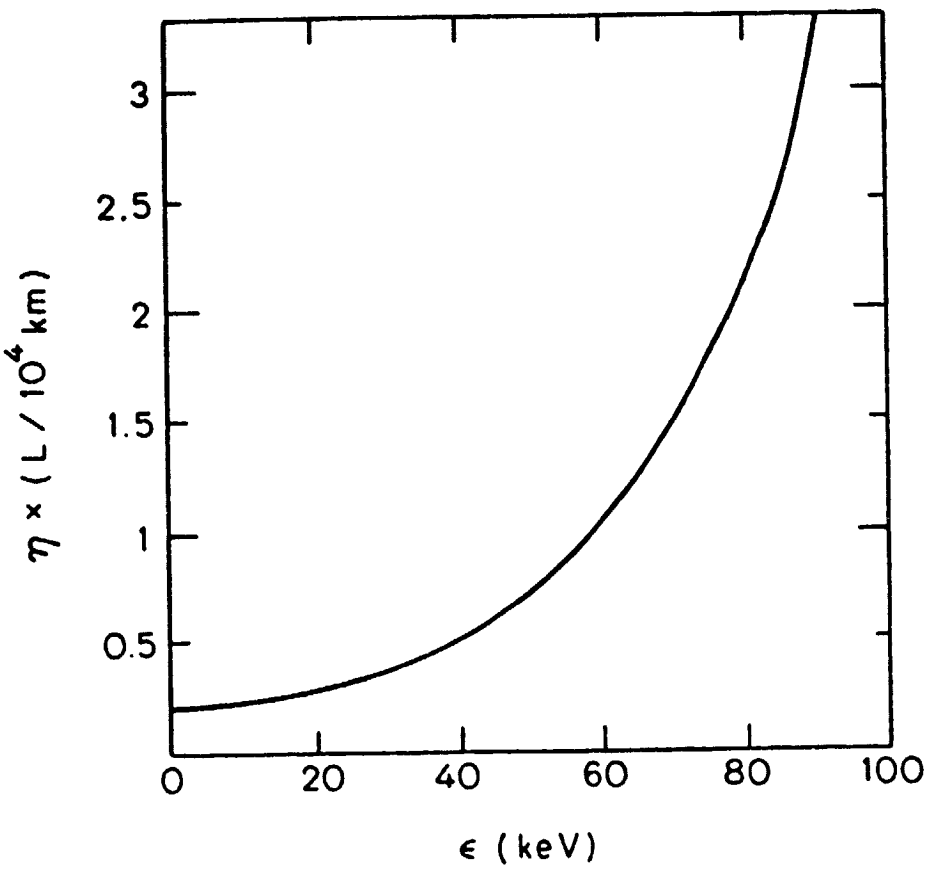

Figure 3

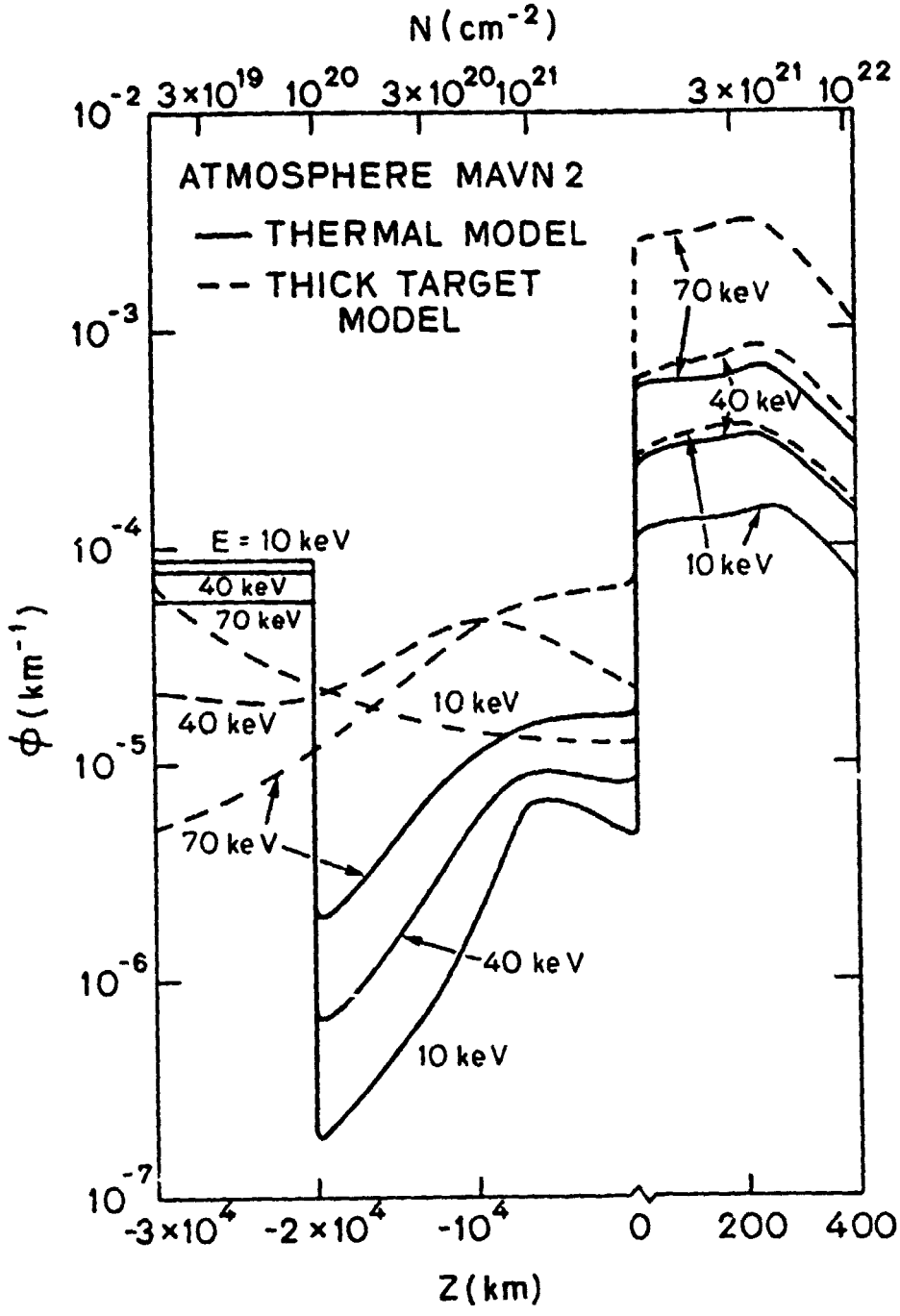
N (cm⁻²)
10⁻² 3×10¹⁹ 10²⁰ 3×10²⁰ 10²¹ 3×10²¹ 10²²
ATMOSPHERE MAVN 2
THERMAL MODEL
THICK TARGET MODEL
70 keV
40 keV
10 keV
E = 10 keV
40 keV
70 keV
10 keV
40 keV
70 keV
40 keV
10 keV
10⁻³
10⁻⁴
10⁻⁵
10⁻⁶
10⁻⁷
φ (km⁻¹)
-3×10⁴ -2×10⁴ -10⁴ 0 200 400
Z (km)

Figure 4